Chemosphere 276 (2021) 130158

Contents lists available at ScienceDirect

Chemosphere

journal homepage: www.elsevier.com/locate/chemosphere

Efficient removal of Congo red using curcumin conjugated zinc oxide nanoparticles as new adsorbent complex

Celine Arab, Riham El Kurdi, Digambara Patra*

Department of Chemistry, American University of Beirut, Beirut, Lebanon

HIGHLIGHTS

- Zinc curcumin oxide nanoparticles were prepared via a green synthesis method.
- Effect of flow rate of KOH, pH, temperature and polymer addition were optimized.
- Adsorption of congo red organic dye was studied using Zn(Cur)O and ZnO NPs.
- The adsorption process was found to follow a pseudo-second order kinetic model.
- The highest adsorption capacity was obtained for Zn(Cur)O nanoparticles.

GRAPHICAL ABSTRACT

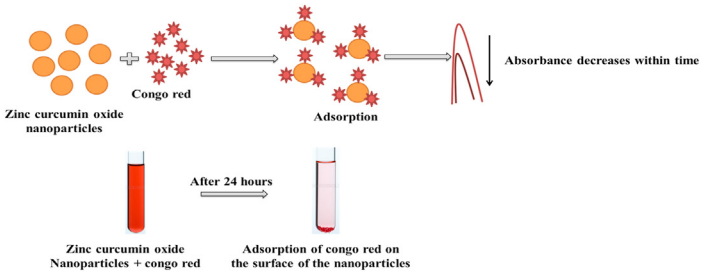

ARTICLE INFO

Article history:
Received 21 November 2020
Received in revised form
25 February 2021
Accepted 27 February 2021
Available online 4 March 2021

Handling Editor: Junfeng Niu

Keywords:
Curcumin
Zn(Cur)O
Removal
Adsorption
Adsorption capacity
Congo red

ABSTRACT

Congo red is one of the common organic dyes that is found in water as waste of the industrial work. The use of congo red has long been of great concern, primarily because of its carcinogenic properties. Congo red can be isolated and removed from water by adsorption using nanoparticles. The use of zinc curcumin oxide, also known as curcumin conjugated zinc oxide, nanoparticles was elaborated for the first time in this work for this purpose. The optimization of the synthesis reaction of zinc curcumin oxide nanoparticles was established by modifying the flow rate of KOH, pH of the medium, different temperature, and in the presence or absence of chitosan polymer. These nanoparticles were characterized through SEM, UV–Visible absorption Spectroscopy, fluorescence spectroscopy, TGA, and XRD. It is found that during synthesis, addition of KOH dropwise in alkaline media improved the stability of the formed nanoparticles. Similarly, addition of chitosan has further increased their stability with only 10% mass loss. The importance of the formed nanoparticles was investigated by analyzing their efficiency in the adsorption of congo red where Zn(Cur)O had an adsorption capacity equal to 89.85 mg/g, which is one of the highest reported in literature, following the pseudo second order model. Nevertheless, negative surface charge of congo red and positive surface charge of Zn(Cur)O may also get supported by $\pi-\pi$ interaction between curcumin and congo red that encourages adsorption in zinc curcumin oxide which is obstructed in the presence of chitosan.

1. Introduction

Nanoparticles (NPs) have several exciting and different physical, chemical and biological properties compared to the bulk materials

* Corresponding author.
E-mail address: dp03@aub.edu.lb (D. Patra).

https://doi.org/10.1016/j.chemosphere.2021.130158
0045-6535/

(Siddiqi et al., 2018) which make them applicable in differenet fields (Ealias & Saravanakumar, 2017). Among metal oxide NPs, zinc oxide (ZnO) NPs are widely investigated and developed (Czyżowska and Barbasz, 2020; Ealias & Saravanakumar, 2017). The synthesis of ZnO NPs could be done through several chemical, physical and biological reaction (Król et al., 2017) resulting from the large ratio of the NPs surface to its volume (Czyżowska and Barbasz, 2020). The structure, morphology and the size of ZnO NPs depends strongly on the synthesis process, salt precursor used, additive reagents, pH, temperature and surface modification (Siddiqi et al., 2018). ZnO may be formed in nanorods shape (Wang and Lou, 2008), nanoplates (Jang et al., 2008), nanospheres and nanosheets (Kakiuchi et al., 2006), nanowires (Ding and Wang, 2009), etc. and these shapes and sizes can influence its properties. ZnO has many characteristics (McClements et al., 2015) which make them useful for application in degradation of environmental pollutants (Cristina Yeber et al., 2000), chemical and biological sensor (Omichi et al., 2001), gas sensors (Xu et al., 2000), solar cells (Jeong et al., 2006), antibacterial devices and medical uses (Rekha et al., 2010).

In another interesting properties, ZnO can be sensitized towards the visible light and can act as a good adsorbent. Doping with organic system or modifying its surface can further improve the adsorption properties of ZnO, which can be carried out by several methods. Surface modification of ZnO by incorporation of fullerenes (Liao et al., 2013), polymers (Hariharan et al., 2012) and organic materials (Qiu et al., 2008) has been reported. Curcumin has been added to the ZnO NPs to form zinc curcumin oxide nanoparticles (Zn(Cur)O NPs) (Moussawi and Patra, 2016b). Curcumin is used as a reducing agent for preparation of metallic NPs (El Kurdi and Patra, 2018; Sreelakshmi et al., 2013) and as a conjugating agent for metal oxide NPs (Haneefa et al., 2017; Moussawi and Patra, 2016a). Zn(Cur)O NPs have been used as antimicrobial probe (Soumya et al., 2017), antimicrobial and antioxidant agent (Jacob and Rajiv, 2019) and for scavenging activity (Nasrallah et al., 2018). Anticancer effect of Zn(Cur)O NPs and their efficiency on cancerous cell have been tested (Perera et al., 2020). Zn(Cur)O has also been used for environmenral applications, such as for adsorption of arsenite (Moussawi and Patra, 2016a) and removal of perylene, fluoranthene, and chrysene (Moussawi and Patra, 2016b). Curcumin also helps in the reduction of organic dye when combined to metal oxide NPs (Abou-Gamra and Ahmed, 2016; Qasem et al., 2020), thus, its conjugation with ZnO NPs could enhance its adsorption activity.

Organic dyes are one of the major concerns as organic pollutants in water. Congo red is one of the relevant organic dyes that is found in water. It is a secondary diazo dye with a complex aromatic structure that makes it non-biodegradable and fairly stable. Congo red can be easily dissolved in water, inducing several difficulties when removing from contaminated water. It is toxic and carcinogenic, and it affects the eyes, skin, respiratory, and reproductive systems. Due to the surface area, surface charge and porosity of zinc oxide, congo red is expected to get adsorbed on its surface. Since shape, stability and crystallinity of ZnO NPs depends on the reaction factors, the present work is aimed for the development and the optimization of the synthesis parameters in order to get the most suitable and efficient Zn(Cur)O NPs. Curcumin at the surface of zinc oxide may further improve adsorption of congo red. Thus, Zn(Cur)O NPs were prepared using various synthetic conditions and the formed nanoparticles were established and elaborated as new adsorbent for the adsorption of congo red. Further modification of Zn(Cur)O NPs was made by coating with chitosan oligosaccharide lactate (chitosan), which were compared with naked ZnO NPs for the adsorption of congo red.

2. Materials and methods

2.1. Materials

Zinc nitrate hexahydrate ($Zn(NO_3)_2.6H_2O$) and congo red (98% extra pure) were acquired from Acros Organics. Curcumin was obtained from Sigma. Potassium hydroxide was received from AnalaR. Acetone (HPLC grade) and chitosan oligosaccharide lactate (chitosan) were received from Aldrich.

2.2. Methods

The preparation of zinc curcumin oxide nanoparticles was carried out at the first place in neutral media, as described in (Moussawi and Patra, 2016a), with some modifications (see Scheme 1). In the first step, 1.48 g of zinc nitrate hexahydrate (Concentration = 0.1 M) were dissolved in 50 mL double distilled water heated at 80 °C. In a second step, 0.18 g of curcumin (Concentration = 0.1 M) were dissolved in 5 mL acetone. Later on, the two solutions were mixed and kept under reflux at 80 °C for 1 h with continuous stirring at 400 rpm. In a next step, 0.11 g of KOH (Concentration = 0.2 M) dissolved in 10 mL of double distilled water heated at 80 °C were added to the mixture and kept under stirring for 5 min. The solution was centrifuged at 4000 rpm and the precipitate was washed 3 times with double distilled water in order to get rid of the unreacted curcumin. Finally, the washed precipitate was kept under freeze dryer for 24 h. The size, shape, crystallinity, etc. depend strongly on the reaction parameters. For

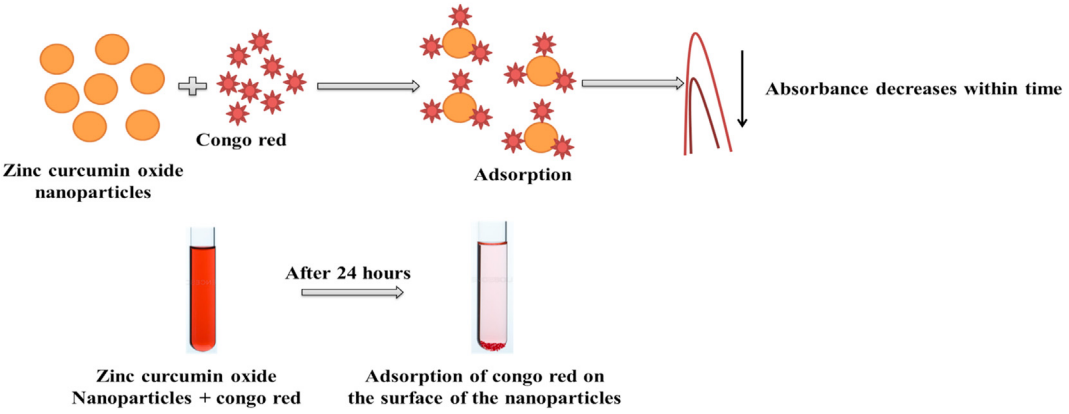

Scheme 1. Adsorption of congo red using zinc curcumin oxide nanoparticles as adsorbent.

this purpose, the reaction parameters were optimized in order to prepare the suitable Zn(Cur)O NPs. Among these parameters, the ones that were tested are the following: flow rate of KOH, pH of the reaction, variation in temperature and addition of a chitosan polymer.

2.2.1. Effect of the flow rate of KOH

A solution of KOH (Concentration = 0.2 M) was prepared by dissolving 0.11 g of KOH in 10 mL double distilled water. It was added to the final solution obtained after reflux by 4 different ways. Accordingly, 4 final solutions were prepared. The first way was the addition of 10 mL KOH directly. In the second solution, this quantity was divided into two part: 5 mL were added using a graduated pipet and the solution was kept under stirring for 2–3 min, then the other 5 mL were added and stirred for the same time interval. The third way was similar to the second one but with the division of the 10 mL into 3 parts (3.33 mL in each step, separated with 30 s of stirring). The last one refers to the addition of the 10 mL KOH drop by drop using a burette while stirring the solution.

2.2.2. Effect of pH

The preparations are similar to the previous ones mentioned above with slightly small changes. After choosing the best way to add KOH, the study of the variation in pH was done to investigate its role in the production of Zn(Cur)O NPs. In this case, the zinc nitrate and the KOH solutions were both prepared in different solutions of pHs equal to 4, 7, 10, and 13 consecutively instead of using double distilled water.

2.2.3. Effect of temperature

After the adoption of the suitable pH, Zn(Cur)O NPs were prepared similarly with variation in temperature, since this parameter is essential and could affect the results in a considerable way. The temperatures used were 40, 60, 80, and 95°*C*.

2.2.4. Effect of polymer addition

Moreover, coating with a polymer was necessary since it improves the results significantly. Chitosan polymer was used for this purpose. Hence, 10 mg of it was added in 3 ways. The first one was its addition directly before reflux. The second way refers to its addition before KOH and the last one was adding chitosan at the end, meaning after adding KOH.

2.3. Characterization technique

The absorption spectra were recorded using a JASCOV-570 UV–vis–NIR Spectrophotometer at room temperature in the range 200–800 nm. The emission fluorescence spectra were recorded at room temperature using Jobin-Yvon-Horiba Fluorolog III fluorometer and the FluorEssence program where the excitation and emission slits width were 5 nm. The source of excitation was a 100 W Xenon lamp, and the used detector was R-928 operating at a voltage of 950 V. For the absorption and fluorescence studies 1 mg of the material were weighed and dissolved in 5 mL of double distilled water heated at 30 °C, which made a dispersion solution. The X-ray diffraction (XRD) data were recorded using a Bruker d8 discover X-ray diffractometer equipped with Cu-Kα radiation (λ = 1.5405 Å). The monochromator used was Johansson type. The step size was 0.02 s and the scan rate was 20 s per step. The Thermogravimetric Analysis (TGA) measurements were done using a Netzsch TGA 209 in the temperature range 0–1000 °*C* with an increment of 30 K/10 min in a N_2 atmosphere. Scanning electron microscopy (SEM) analysis was done using Tescan, Vega 3 LMU with Oxford EDX detector (Inca XmaW20). In short, Zn(Cur)O powder were deposited on an aluminum stub and coated with carbon conductive adhesive tape.

2.4. Adsorption of Congo red

The experiments were done by dissolving 1 mg of ZnO, Zn(Cur)O, and Zn(Cur)O-Chitosan NPs separately in 1 mL of heated double distilled water using a sonicator, and dissolving 3.48 mg of congo red organic dye in 5 mL double distilled water (Concentration = 1 mM). At the beginning, 50 μL (Concentration = 16.5 μM) of the congo red solution was taken and added to 150 μL (150 μg/mL) of ZnO, Zn(Cur)O, and Zn(Cur)O-Chitosan NPs consecutively with 2.8 mL of double distilled water in order to have a total volume equal to 3 mL. The absorbance was measured using UV–Visible spectrophotometer to compare the efficiency of the three types of nanoparticles for intervals of time (t = 0, 5, 10, 20, 30, 40, 60, 80, 110 min, and after 24 h).

3. Results and discussion

3.1. Optimization of the reaction parameters

Since synthetic conditions can change properties of Zn(Cur)O NPs by varying its shape, size, crystalinity and defects, the reaction parameters were optimized in order to prepare the suitable Zn(Cur)O NPs. As described in section 2.2, different optimizations were established and the obtained Zn(Cur)O were compared and characterized through UV–Visible absorption spectroscopy, fluorescence spectroscopy, TGA and XRD.

3.2. Effect of the flow rate of KOH

UV–Visible absorption spectroscopy was used initially in order to characterize the obtained products from the four different trials at 80 °C. Generally, ZnO absorbs at ~360–370 nm and curcumin strongly absorbs at ~425 nm. In case of Zn(Cur)O nanoparticles, as shown in Figure S1A (see Supporting Information, SI), no major peak was observed at ~360–370 nm indicating weak absorption in this region compared to other predominant peak at > 420 nm, which is due to Zn-curcumin interaction or one can say due to defects in ZnO. Interestingly, the curcumin peak was red shifted to higher wavelength when Zn(Cur)O nanoparticles were formed after the addition of KOH solution in 2 steps, 5 mL each, or 3 steps, 3.33 mL each. No remarkable change was observed when adding KOH in one step, 10 mL directly using a pipet. Addition of KOH solution drop by drop using a burette caused the occurrence of a slight blue shift relieving the formation of smaller NPs. This observation could be due to fact that when KOH was added in 2 or 3 steps, the pH of the solution changes to basic medium in the first step and makes free curcumin deprotonated (curcumin has 3 pKa's at pH > 8), in the second and third steps these deprotonated form of curcumin reacts with available Zn^{2+} ions during nucleation process for the further growth of Zn(Cur)O nanoparticles, whereas when KOH was added drop wise or in one step Zn^{2+} reacts with neutral form of curcumin during formation as well as further growth of Zn(Cur)O nanoparticles. The slight blue shift when KOH was added drop wise compared to in one step could be due to difference defects created in Zn(Cur)O nanoparticles during nucleation process because of slower reaction while adding KOH drop wise, this may also encourage more curcumin to get conjugated with ZnO.

As for the fluorescence study, free curcumin exhibits an emission wavelength maximum at around 550 nm (Figure S1B, See SI). This wavelength was red shifted to higher wavelength when curcumin is complexed to ZnO NPs. When adding directly 10 mL of KOH in one step, this peak was slightly shifted to 540 nm with a decrease in the emission intensity. Similalry, when adding the KOH

in 2 or 3 steps, or drop wise this peak red shifted to ~600 nm. This variation is due to different kinds of defects created in ZnO during synthesis of Zn(Cur)O nanoparticles. When KOH was added drop wise, the fluorescence emission maximum shifted to blue slightly compared to when KOH was added in 2 or 3 steps. This is similar to what was found in UV−visible absorption spectrum. The variation of fluorescene intensity suggests greater number of defects when KOH was added drop wise as the reaction process was slower. This can also suggest greater amount of curcumin conjugation as found later on in TGA.

The X-Ray Diffraction (XRD) analysis was also done and the results are depicted in Figure S2A (see SI). The characteristic peaks of curcumin alone appeared at diffraction angles of 2θ equal to 8.06°, 9.14°, 12.37°, 15.06° and 17.75° indicating that curcumin is present in the crystalline form. Curcumin characteristic peaks were slightly present in the Zn(Cur)O NPs X-Ray pattern in the four different cases, meaning that curcumin is conjugated or complexed with ZnO nanoparticles in their crystalline form. As for the experiments where the flow rate of KOH was added using burette (drop wise) or in direct way 10 mL instantly, Zn(Cur)O peaks were somehow observed better than the other two cases. To sum up, curcumin peaks were less prominent in all cases, but new peaks were noticed at 2θ equal to 33° and 34.9° and 58° when adding KOH drop by drop. These new peaks correspond to different kinds of defects generated in Zn(Cur)O nanoparticles.

In addition, based on the thermogravimetric analysis TGA, the percentage of the mass loss with increasing temperature was found lesser for the NPs formed when the burette was used than the other experiments (Figure S2B, see SI). The TGA analysis showed a weight loss in two steps at 210 °C and 430°C. The weight loss is attributed to the decomposition of curcumin. We assume that the difference percentage of mass loss of free curcumin and Zn(Cur)O is due to the degradation path of free curcumin compared to when it is conjugated with ZnO nanoparticles as observed earlier (Nata et al., 2014). Approximatively, Zn(Cur)O NPs prepared in all cases undergo the same degradation. The TGA results indicate that a mass loss of ~80% happened during the thermal breakdown of Zn(Cur)O NPs prepared using a burette for the addition of KOH, and a mass loss of ~85% occurred during the thermal decomposition of the other nanoparticles. The lowest mass loss occurred when using the burette (drop wise) suggests greater amount of curcumin present in this case which is consistent with higher fluorescence intensity observed earlier. Therefore, this condition where KOH is added drop by drop using a burette was used for further study.

3.3. Effect of pH

It is known that curcumin is slightly soluble in water and acidic media but soluble in basic media (at higher pH). Earlier studies have shown that curcumin complexation to ZnO NPs is more stable at higher pH, in alkaline solution, where less than 6% of curcumin was lost after incubation (Peng et al., 2018). For this reason, zinc nitrate was dissolved in different solutions of curcumin in various pHs (4, 7, 10 and 13) and heated at 80°C. The solutions were kept under reflux for 1 h at 80°C and 10 mL of KOH were added drop by drop using a burette. As it is shown in Fig. 1A, the highest absorbance was obtained at pH = 10 and pH = 13 with a slight red shift of the wavelength maximum. However, at pH = 4 and pH = 7, the maximum wavelength did not change compared to the curcumin peak.

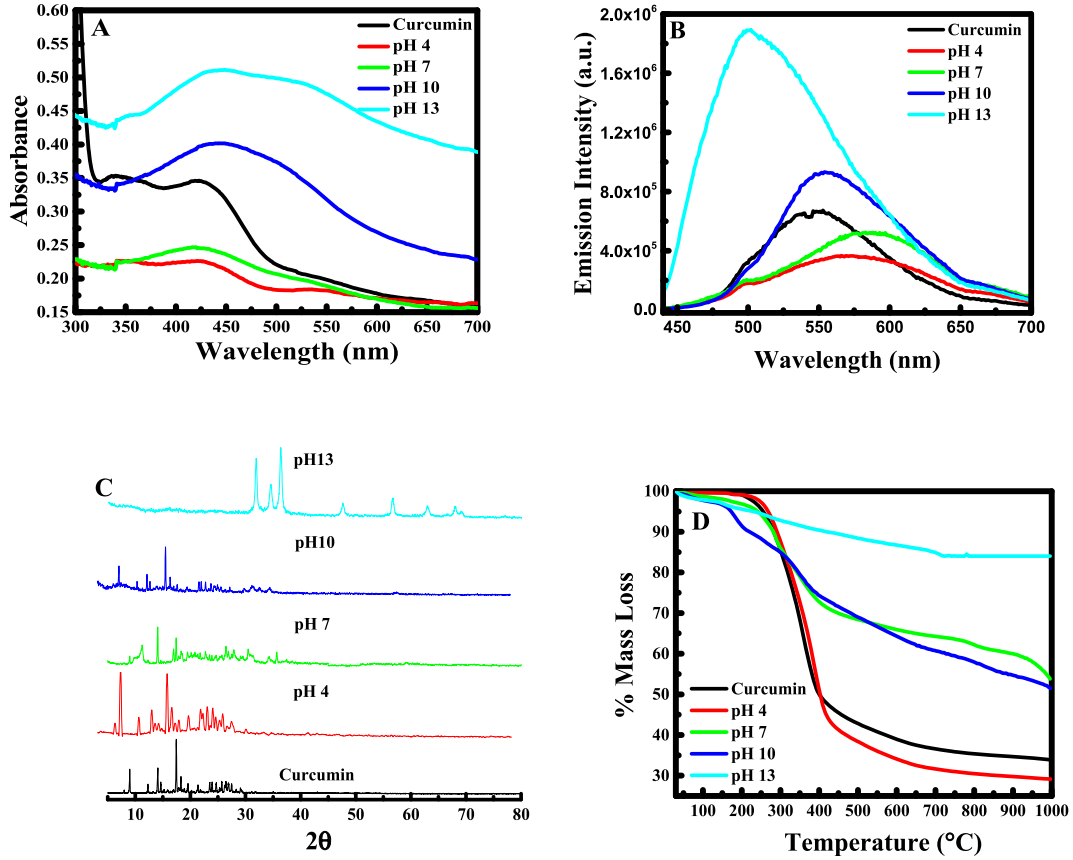

Fig. 1. (A) UV−Visible absorption spectra, (B) fluorescence spectra, (C) X-Ray Diffractogram pattern and (D) Thermogravimetric analysis of curcumin and Zn(Cur)O prepared at different pH.

Moreover, the fluorescence spectrum was recorded and illustrated in Fig. 1B. As it is shown, Zn(Cur)O NPs prepared at pH = 4 have the lowest fluorescence intensity. The fluorescence intensity increased with the increase of the solution pH during preparation, but the fluorescence maximum showed a blue shift to 500 nm at pH = 13. This difference could be due to a defect site that is completely different from the one made in neutral or acidic conditions. The highest fluorescence intensity for this case also suggests greater number of curcumin conjugation. More number of hydrophobic curcumin around each other changes the microenvironment from completely polar/aqueous to less polar environment, which may shift the fluorescence maximum to lower wavelength, which is in consistent with earlier shift in Figure S2B (see SI).

These samples were further verified by XRD diffractogram, where the characteristic peak of Zn(Cur)O NPs were remarkably observed only at pH = 13 at 2θ values equal to 31.63° (hkl, 100), 34.45° (hkl, 002), 36.32° (hkl, 101), 47.45° (hkl, 102), 56.66° (hkl, 110), 63.02° (hkl, 103), 67.87° (hkl, 112) and 69.25° (hkl, 201). These diffraction peaks indicate the formation of a hexagonal wurtzite structure. These results were similarly obtained with Nasrallah et al. and Soumya et al. (Nasrallah et al., 2018; Soumya et al., 2017). Interestingly, curcumin diffraction peak were totally disappeared indicating that curcumin has been complexed to ZnO completely (Fig. 1C). In contrast, curcumin XRD peaks were obtained for samples prepared at pHs 4, 7 and 10, meaning that all the curcumin molecules did not react to form Zn(Cur)O NPs. Finally, looking at the results of the TGA illustrated in Fig. 1D, no degradation of curcumin was observed and a high stability for the Zn(Cur)O was obtained with < 20% loss in mass at pH = 13. The highest percentage of mass loss was observed for pH = 4 (the most acidic) and it is approximately equal to 70%. In addition, Zn(Cur)O NPs prepared at pH = 7 and pH = 10 had a mass loss of about 45%. This is also consistent with our earlier TGA results that higher curcumin conjugation gives less mass loss. In conclusion, based on the analysis done above, pH = 13 was found to be the most suitable for the formation of zinc curcumin oxide nanoparticles.

3.4. Effect of temperature

The reaction temperature was varied from 40 to 95°C. When the temperature was increased from 40 to 80°C, more curcumin has reacted allowing the formation of more Zn(Cur)O NPs, as shown in Fig. 2A where the absorbance increases. The same applies for the fluorescence intensity that increases with the temperature as well (Fig. 2B), except for the highest temperature, 95°C, where both the absorbance and emission intensities decreased with slight red shift in the UV–Visible absorption peak, this small change could be new defect site at higher temperature due to less amount of curcumin conjugation. As for the X-Ray Diffraction analysis (Fig. 2C), the patterns for the lowest two temperatures 40 and 60 °C indicate the presence of only two characteristic peaks for Zn(Cur)O NPs implying the occurrence of an incomplete reaction inhibiting the formation of Zn(Cur)O NPs. However, the XRD patterns of 80 and 95°C represent the characteristic peaks of Zn(Cur)O nanoparticles,

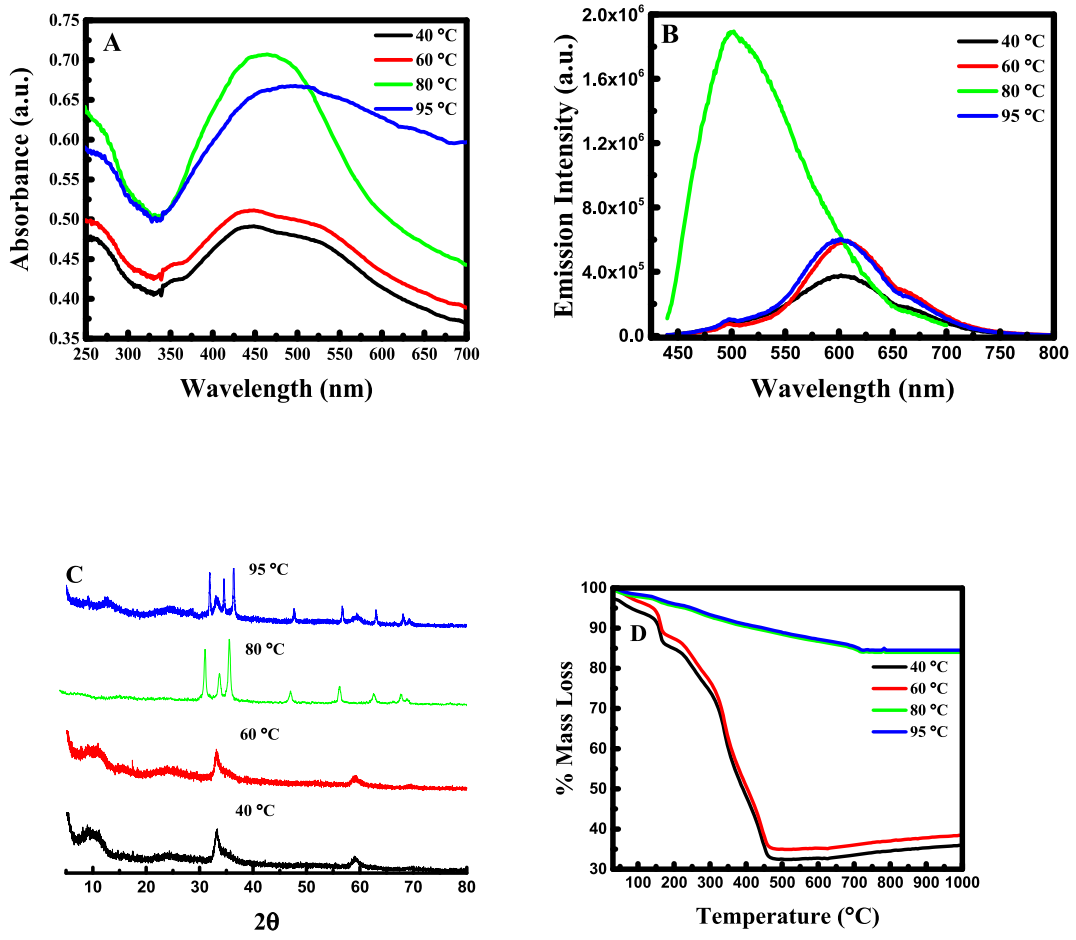

Fig. 2. (A) UV–Visible absorption spectra, (B) fluorescence spectra, (C) X-Ray Diffractogram pattern and (D) Thermogravimetric analysis of Zn(Cur)O prepared at different temperature.

meaning that at high temperature curcumin can be easily complexed to ZnO NPs. TGA results (see Fig. 2D) indicate a significant mass loss of around 70% and 65% at 40 and 60°*C* respectively, which suggests the presence of free curcumin with no complete formation of Zn(Cur)O NPs confirming the XRD results. However, at 80 and 95°*C*, the mass loss is around 15% indicating a better interaction and complexation of curcumin with ZnO NPs, which further confirms results obtained from XRD. As a result, 80°*C* is the most appropriate temperature to be used according to the optimization studies, preventing furthermore the boiling of water during the reflux at higher temperatures.

3.5. Effect of polymer addition

Coating Zn(Cur)O NPs may prevent the formation of clusters (Nasrallah et al., 2018; Peng et al., 2018; Soumya et al., 2017). It will be proven that it also increases the stability of Zn(Cur)O NPs. The addition of chitosan was monitored in 3 different ways, after or before the addition of KOH, or before the start of the reflux. As it is noticed from the UV–Visible absorption and fluorescence spectra presented in Figures S3A and S3B (see SI), the UV–visible absorption peak at 360–370 nm became prominent when adding chitosan compared to the Zn(Cur)O NPs prepared without coating suggesting chistoan directly gets involved during the formation of ZnO and creates different defect sites than Zn(Cur)O but similar to naked ZnO. Though curcumin absorption peak is weak, the fluorescence spectra confirm curcumin conjugation. The highest fluorescence intensity was obtained for the case when chitosan was added after KOH compare to when chitosan was added before KOH. This suggests chitosan competes with curcumin for conjugation during the formation of Zn(Cur)O when chitosan is added before KOH by forming particles which are similar to naked ZnO. At the same time when chitosan is added after KOH some curcumin are already conjugated with Zn(Cur)O.

Furthermore, the XRD pattern was established and shown in Figure S4A (see SI). Same characteristic peaks were obtained in all cases compared to the Zn(Cur)O prepared without chitosan. The relative characteristics peak are 31.63°, 34.45°, 36.32°, 47.45°, 56.66°, 63.02°, 67.87° and 69.25°. This means that the addition of chitosan did not alter the crystallinity of Zn(Cur)O NPs. As for TGA, it is well noticed that less than 10% of mass loss was occurred when adding chitosan, compared to the NPs prepared without chitosan. This further clarifies less amount of curcumin conjugation in the presence of chitosan and confirms the role of chitosan as a coating layer increasing the stability (less mass loss) of the formed nanoparticles (See Figure S4B, see SI). To sum up, since no remarkable difference was obtained in XRD and UV–visible absoprtion spectrum between the three different ways of adding the polymer, chitosan added after KOH was considered in the applications since it has greater amount of curcumin conjugation (highest fluorescence intensity was obtained). The final zinc curcumin oxide nanoparticles in absence and presence of chitosan were characterized through SEM to identify their shape. The SEM images are presented in Fig. 3A&B. Interestingly, in both cases spheres NPs were obtained verifying the role of chitosan as a stabilizing agent and do not affect the composition and the shape of Zn(Cur)O NPs.

3.6. Adsorption of Congo red

After mixing 150 μL of ZnO, Zn(Cur)O, and Zn(Cur)O-Chitosan NPs, with 50 μL of congo red organic dye and 2.8 mL of double distilled water, the absorbance was measured using UV–Visible spectrophotometer. The experiment was done at different intervals of time (t = 0, 5, 10, 20, 30, 40, 60, 80, 110 min, and 24 h). Fig. 4A presents the UV–Visible absorption spectrum of congo red within time in the presence of Zn(Cur)O. As observed in Fig. 4A, a decrease in the absorbance was obtained within time. The adsorption capacity was calculated based on the equation below:

$$q_e = \frac{(C_0 - C_e)V}{m} \quad (1)$$

where C_0 and C_e are the initial concentration and the equilibrium concentration of congo red respectively (mg/L), V is the volume of the solution (mL) and m is the mass of Zn(Cur)O NPs (g). It was found that the q_e in this case was equal to 89.85 mg/g which is relatively high compared to previous method used in the literature (See Table 1). The high adsorption capacity was also confirmed visually, as after 24 h the solution color turned from dark red to almost transparent, where the congo red and the zinc curcumin oxide nanoparticles settled down. This precipitation indicates that all the congo red molecules have been adsorbed. Furthermore, the effect of stirring was also investigated. For this purpose, in a first place the mixtures were kept under stirring during measurement at 200 rpm and in a 2nd place the experiment was done using water

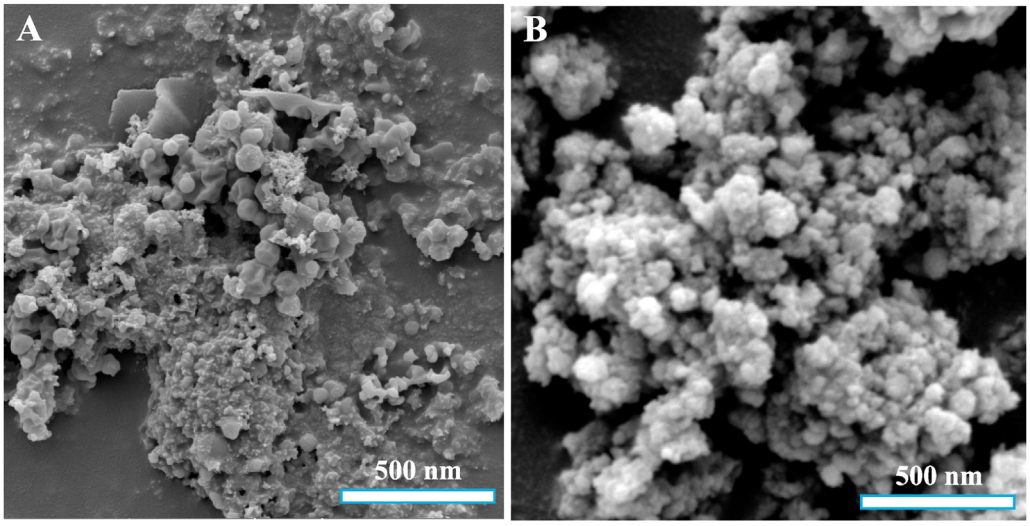

Fig. 3. (A) SEM image of Zn(Cur)O NPs and (B) SEM image of Zn(Cur)O NPs coated with chitosan.

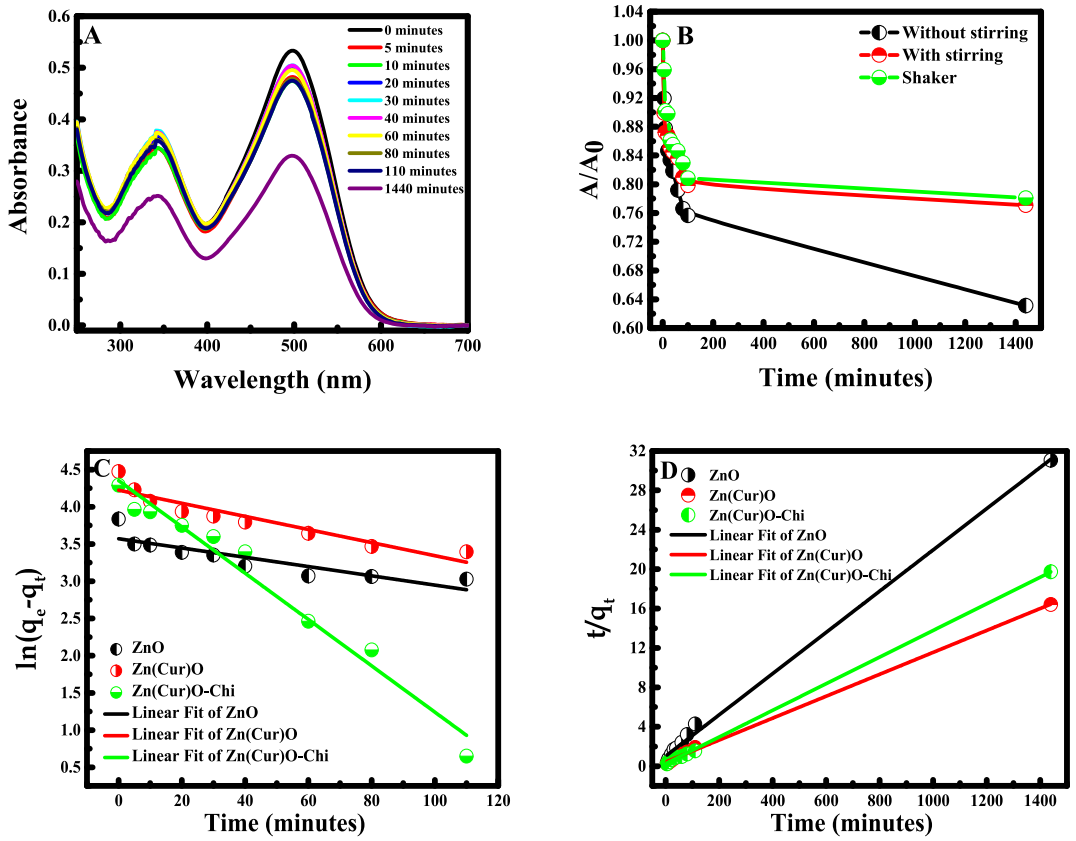

Fig. 4. (A) UV–Visible absorption spectra of Congo red in the presence of Zn(Cur)O, (B) A/A_0 of Congo red in the presence of Zn(Cur)O without/with stirring and using shaker, (C) pseudo first order kinetic model and (D) pseudo second order kinetic model adsorption of Congo red in the presence of Zn(Cur)O. (For interpretation of the references to color in this figure legend, the reader is referred to the Web version of this article.)

Table 1
Different methods used to adsorb congo red.

Adsorbent	Concentration of adsorbent (g/L)	Concentration of Congo Red (mg/L)	Kinetic order	q_e (exp) (mg/g)	R^2	Reference
Mesoporous α-Fe_2O_3 nanorods	1	20	Pseudo-second order	18.7	0.99	Maiti et al. (2017)
Porous soybean curd xerogels	1.25	40	Pseudo-second order	27.46	0.99	Zhang et al. (2018)
Activated carbon coffee waste	4	20	Pseudo-second order	9.41	0.99	Lafi et al. (2019)
Zn(Cur)O	0.15	11.15	Pseudo-second order	89.85	0.99	Our work

bath shaker at 200 rpm also. As depicted in Fig. 4B, A/A_0 ratio decreases faster. Meaning that, the high adsorption was obtained when the reaction occurred without stirring. The q_e value in the three cases was equal to 89.85 mg/g, 8.66 mg/g, 5.30 mg/g without stirring, with stirring and using shaker respectively. Hence, the adsorption capacity was found to be higher when keeping the solution undisturbed, meaning that congo red molecule can be easily adsorbed on the surface of Zn(Cur)O.

Moreover to establish the efficiency of Zn(Cur)O NPs as adsorbent of congo red, the adsoption study was done using ZnO NPs and Zn(Cur)O-Chitosan. In order to understand the adsorption kinetics of the three adsorbents, the pseudo-first order and pseudo-second order kinetic models were plotted using the following equations respectively:

$$\ln(q_e - q_t) = \ln(q_e) - k_1 t \quad (2)$$

$$\frac{t}{q_t} = \frac{1}{k_2 q_e^2} + \frac{1}{q_e} t \quad (3)$$

where q_t and q_e are the adsorption capacity at time t and at equilibrium respectively (mg/g), t is the time (min), k_1 is the rate constant of the pseudo-first order model (min^{-1}), and k_2 is the rate constant of the pseudo-second order model ($g.mg^{-1}.min^{-1}$).

Congo red adsorption was presented for the pseudo-first order and pseudo-second order in Fig. 4C&D respectively. A linear curve was obtained for the pseudo-first order model where the values of q_e and k_1 are calculated from the intercept and slope, respectively. Similarly, a linear curve was obtained for the pseudo-second order model where q_e is calculated from the slope and k_2 from the intercept (See Table 2). Based on the collected information, a remarkable difference in the R^2 values was obtained for both orders where the R^2 value was higher when fitting with the pseudo second order. Furthermore, the experimental adsorption capacity values of the pseudo-second order kinetic model were closer to the calculated value of q_e for the three types of adsorbents, confirming that the process follows second order kinetics (Madan et al., 2019; Pratiwi et al., 2018).

After choosing the pseudo-second order model as the most suitable one, the best adsorbent could be selected. Comparing the values of q_e, the adsorption capacity, it could be noticed that the

Table 2
Kinetic parameters of the pseudo-first order and pseudo-second order models.

Adsorbent	Pseudo-first order			Pseudo-second order			q_e (calc)
	q_e (exp)	k1	R^2	q_e (exp)	k2	R^2	
ZnO	35.56	0.0062	0.74	47.78	0.00043	0.99	46.35
Zn(Cur)O	68.26	0.0088	0.86	89.85	0.00039	0.99	87.70
Zn(Cur)O-Chitosan	77.60	0.0311	0.96	73.96	0.00080	0.99	72.94

best adsorbent is Zn(Cur)O, followed by Zn(Cur)O-Chitosan, then ZnO nanoparticles. This could be explained by the interaction between congo red and curcumin as negative surface charge of congo red and positive surface charge of Zn(Cur)O may also get supported by $\pi-\pi$ interaction between curcumin and congo red, however, this interaction is masked by chitosan polymer in Zn(Cur)O-Chitosan NPs, and not present at all in ZnO NPs.

4. Conclusion

In conclusion, Zn(Cur)O NPs were synthesized through a simple method in the presence of curcumin. It was found that the flow rate of KOH has a significant effect on the formation of Zn(Cur)O NPs. In addition, during the formation of Zn(Cur)O NPs, curcumin conjugation increased at pH = 13 and at 80°C. Furthermore, the stability of these NPs was increased when coating the formed NPs with chitosan. The obtained Zn(Cur)O NPs nanoparticles showed a high adsorption capacity of congo red organic dye onto their surface following the pseudo second order model and using only 0.15 g/L of Zn(Cur)O NPs compared to ZnO and Zn(Cur)O-Chitosan. Intrestingly, negative surface charge of congo red and positive surface charge of Zn(Cur)O is supported by $\pi-\pi$ interaction between curcumin and congo red, however, this interaction is masked by chitosan in Zn(Cur)O-Chitosan NPs, and not present at all in ZnO NPs that decreased adsorption of congo red.

Author statement

Celine Arab: Methodology, Formal analysis, Investigation, Experiment, Validation, Writing – original draft; Riham El Kurdi: Formal analysis, Experiment, Analysis, Writing- Reviewing and Editing. Digambara Patra: Conceptualization, Supervision, Resources, Project administration, Writing- Reviewing and Editing.

Declaration of competing interest

The authors declare that they have no known competing financial interests or personal relationships that could have appeared to influence the work reported in this paper.

Acknowledgments

Financial support provided by American University of Beirut, Lebanon through University Research Board (URB) as well as Kamal A. Shair Central Research Laboratory (KAS CRSL) facilities to carry out this work is greatly acknowledged.

Appendix A. Supplementary data

Supplementary data to this article can be found online at https://doi.org/10.1016/j.chemosphere.2021.130158.

References

Abou-Gamra, Z.M., Ahmed, M.A., 2016. Synthesis of mesoporous TiO2-curcumin nanoparticles for photocatalytic degradation of methylene blue dye. J. Photochem. Photobiol. B Biol. 160, 134–141. https://doi.org/10.1016/j.jphotobiol.2016.03.054.

Cristina Yeber, M., Rodriguez, J., Freer, J., Duran, N., D Mansilla, H., 2000. Photocatalytic degradation of cellulose bleaching effluent by supported TiO2 and ZnO. Chemosphere 41 (8), 1193–1197. https://doi.org/10.1016/S0045-6535(99)00551-2.

Czyżowska, A., Barbasz, A., 2020. A review: zinc oxide nanoparticles–friends or enemies? Int. J. Environ. Health Res. 1–17. https://doi.org/10.1080/09603123.2020.1805415.

Ding, Y., Wang, Z.L., 2009. Structures of planar defects in ZnO nanobelts and nanowires. Micron 40 (3), 335–342. https://doi.org/10.1016/j.micron.2008.10.008.

Ealias, A.M., Saravanakumar, M.P., 2017. A review on the classification, characterisation, synthesis of nanoparticles and their application. IOP Conf. Ser. Mater. Sci. Eng. 263, 1–15. https://doi.org/10.1088/1757-899X/263/3/032019.

El Kurdi, R., Patra, D., 2018. Tuning the surface of Au nanoparticles using poly(-ethylene glycol)- block -poly(propylene glycol)- block -poly(ethylene glycol): enzyme free and label free sugar sensing in serum samples using resonance Rayleigh scattering spectroscopy. Phys. Chem. Chem. Phys. 20 (14), 9616–9629. https://doi.org/10.1039/c8cp01147h.

Haneefa, M.M., Jayandran, M., Balasubramanian, V., 2017. Evaluation of antimicrobial activity of green-synthesized manganese oxide nanoparticles and comparative studies with curcuminaniline functionalized nanoform. Asian J. Pharmaceut. Clin. Res. 10 (3), 347–352. https://doi.org/10.22159/ajpcr.2017.v10i3.16246.

Hariharan, R., Senthilkumar, S., Suganthi, A., Rajarajan, M., 2012. Photodynamic action of curcumin derived polymer modified ZnO nanocomposites. Mater. Res. Bull. 47 (11), 3090–3099. https://doi.org/10.1016/j.materresbull.2012.08.028.

Jacob, V., Rajiv, P., 2019. IN vitro ANALYSIS : the antimicrobial and antioxidant activity OF zinc oxide nanoparticles from curcuma longa. Asian J. Pharmaceut. Clin. Res. 12 (1), 200–204.

Jang, J.S., Yu, C.J., Choi, S.H., Ji, S.M., Kim, E.S., Lee, J.S., 2008. Topotactic synthesis of mesoporous ZnS and ZnO nanoplates and their photocatalytic activity. J. Catal. 254 (1), 144–155. https://doi.org/10.1016/j.jcat.2007.12.010.

Jeong, W.J., Kim, S.K., Park, G.C., 2006. Preparation and characteristic of ZnO thin film with high and low resistivity for an application of solar cell. Thin Solid Films 506, 180–183. https://doi.org/10.1016/j.tsf.2005.08.213.

Kakiuchi, K., Hosono, E., Kimura, T., Imai, H., Fujihara, S., 2006. Fabrication of mesoporous ZnO nanosheets from precursor templates grown in aqueous solutions. J. Sol. Gel Sci. Technol. 39 (1), 63–72. https://doi.org/10.1007/s10971-006-6321-6.

Król, A., Pomastowski, P., Rafińska, K., Railean-Plugaru, V., Buszewski, B., 2017. Zinc oxide nanoparticles: synthesis, antiseptic activity and toxicity mechanism. Adv. Colloid Interface Sci. 249, 37–52. https://doi.org/10.1016/j.cis.2017.07.033.

Lafi, R., Montasser, I., Hafiane, A., 2019. Adsorption of Congo red dye from aqueous solutions by prepared activated carbon with oxygen-containing functional groups and its regeneration. Adsorpt. Sci. Technol. 37 (1–2), 160–181. https://doi.org/10.1177/0263617418819227.

Liao, S.H., Jhuo, H.J., Cheng, Y.S., Chen, S.A., 2013. Fullerene derivative-doped zinc oxide nanofilm as the cathode of inverted polymer solar cells with low-bandgap polymer (PTB7-Th) for high performance. Adv. Mater. 25 (34), 4766–4771. https://doi.org/10.1002/adma.201301476.

Madan, S., Shaw, R., Tiwari, S., Tiwari, S.K., 2019. Adsorption dynamics of Congo red dye removal using ZnO functionalized high silica zeolitic particles. Appl. Surf. Sci. 487, 907–917. https://doi.org/10.1016/j.apsusc.2019.04.273.

Maiti, D., Mukhopadhyay, S., Devi, P.S., 2017. Evaluation of mechanism on selective, rapid, and superior adsorption of Congo red by reusable mesoporous α-Fe2O3 nanorods. ACS Sustain. Chem. Eng. 5 (12), 11255–11267. https://doi.org/10.1021/acssuschemeng.7b01684.

McClements, D.J., Li, F., Xiao, H., 2015. The nutraceutical bioavailability classification scheme: classifying nutraceuticals according to factors limiting their oral bioavailability. Annual Review of Food Science and Technology 6 (1), 299–327. https://doi.org/10.1146/annurev-food-032814-014043.

Moussawi, R.N., Patra, D., 2016a. Modification of nanostructured ZnO surfaces with curcumin: fluorescence-based sensing for arsenic and improving arsenic removal by ZnO. RSC Adv. 6 (21), 17256–17268. https://doi.org/10.1039/c5ra20221c.

Moussawi, R.N., Patra, D., 2016b. Nanoparticle self-assembled grain like curcumin conjugated ZnO: curcumin conjugation enhances removal of perylene, fluoranthene, and chrysene by ZnO. Sci. Rep. 6 (1), 1–13. https://doi.org/10.1038/srep24565.

Nasrallah, O., El Kurdi, R., Mouslmani, M., Patra, D., 2018. Doping of ZnO

nanoparticles with curcumin: pH dependent release and DPPH scavenging activity of curcumin in the nanocomposites. Current Nanomaterials 3 (3), 147–152. https://doi.org/10.2174/2405461503666181116115755.
Nata, I.F., Chen, K.J., Lee, C.K., 2014. Facile microencapsulation of curcumin in acetylated starch microparticles. J. Microencapsul. 31 (4), 344–349. https://doi.org/10.3109/02652048.2013.858789.
Omichi, K., Kaiya, K., Takahashi, N., Nakamura, T., Okamoto, S., Yamamoto, H., 2001. Growth of ZnO thin films exhibiting room-temperature ultraviolet emission by means of atmospheric pressure vapor-phase epitaxy. J. Mater. Chem. 11 (2), 262–263. https://doi.org/10.1039/b006656g.
Peng, S., Li, Z., Zou, L., Liu, W., Liu, C., McClements, D.J., 2018. Improving curcumin solubility and bioavailability by encapsulation in saponin-coated curcumin nanoparticles prepared using a simple pH-driven loading method. Food and Function 1829–1839. https://doi.org/10.1039/c7fo01814b.
Perera, W.P.T.D., Dissanayake, R.K., Ranatunga, U.I., Hettiarachchi, N.M., Perera, K.D.C., Unagolla, J.M., De Silva, R.T., Pahalagedara, L.R., 2020. Curcumin loaded zinc oxide nanoparticles for activity-enhanced antibacterial and anti-cancer applications. RSC Adv. 10 (51), 30785–30795. https://doi.org/10.1039/d0ra05755j.
Pratiwi, M.I., Afifah, N., Saleh, R., 2018. Adsorption of organic cationic dye into Fe-doped ZnO nanoparticle coupled with montmorillonite adsorbent. In: AIP Conference Proceedings, vol. 2023, pp. 1–5. https://doi.org/10.1063/1.5064020, 1.
Qasem, M., El Kurdi, R., Patra, D., 2020. Green synthesis of curcumin conjugated CuO nanoparticles for catalytic reduction of methylene blue. Chemistry 5 (5), 1694–1704. https://doi.org/10.1002/slct.201904135.
Qiu, R., Zhang, D., Mo, Y., Song, L., Brewer, E., Huang, X., Xiong, Y., 2008. Photocatalytic activity of polymer-modified ZnO under visible light irradiation. J. Hazard Mater. 156 (1–3), 80–85. https://doi.org/10.1016/j.jhazmat.2007.11.114.
Rekha, K., Nirmala, M., Nair, M.G., Anukaliani, A., 2010. Structural, optical, photocatalytic and antibacterial activity of zinco xide and manganese doped zinc oxide nanoparticles. Phys. B Condens. Matter 405 (15), 3180–3185. https://doi.org/10.1016/j.physb.2010.04.042.
Siddiqi, K.S., ur Rahman, A., Tajuddin, Husen, A., 2018. Properties of zinc oxide nanoparticles and their activity against microbes. Nanoscale Research Letters 13 (1), 1–13. https://doi.org/10.1186/s11671-018-2532-3.
Soumya, K.R., Snigdha, S., Sugathan, S., Mathew, J., Radhakrishnan, E.K., 2017. Zinc oxide–curcumin nanocomposite loaded collagen membrane as an effective material against methicillin-resistant coagulase-negative Staphylococci. 3 Biotech 7 (238), 1–10. https://doi.org/10.1007/s13205-017-0861-z.
Sreelakshmi, C., Goel, N., Datta, K.K.R., Addlagatta, A., Ummanni, R., Reddy, B.V.S., 2013. Green synthesis of curcumin capped gold nanoparticles and evaluation of their cytotoxicity. Nanosci. Nanotechnol. Lett. 5, 1–8. https://doi.org/10.1166/nnl.2013.1678.
Wang, T.X., Lou, T.J., 2008. Solvothermal synthesis and photoluminescence properties of ZnO nanorods and nanorod assemblies from ZnO2 nanoparticles. Mater. Lett. 62 (15), 2329–2331. https://doi.org/10.1016/j.matlet.2007.11.083.
Xu, J., Pan, Q., Shun, Y., Tian, Z., 2000. Grain size control and gas sensing properties of ZnO gas sensor. Sensor. Actuator. B Chem. 66 (1), 277–279. https://doi.org/10.1016/S0925-4005(00)00381-6.
Zhang, Z., Li, Y., Du, Q., Li, Q., 2018. Adsorption of Congo red from aqueous solutions by porous soybean curd xerogels. Pol. J. Chem. Technol. 20 (3), 95–102. https://doi.org/10.2478/pjct-2018-0044.